Jakub Čížek[a], Ivan Procházka[a], Bohumil Smola[a], Ivana Stulíková[a], Martin Vlach[a], Vladivoj Očenášek[b], Olya B. Kulyasova[c], Rinat K. Islamgaliev[c]

[a] Faculty of Mathematics and Physics, Charles University in Prague, Czech Republic
[b] Research Institute of Metals, Panenské Břežany, Czech Republic
[c] Institute of Physics of Advanced Materials, Ufa State Aviation Technical University, Ufa, Russia

Precipitation effects in ultra-fine-grained Mg–RE alloys

Mg-based alloys with rare-earth alloying elements are promising hardenable lightweight materials with good mechanical properties even at elevated temperatures. Ductility and strength of these alloys can be improved by grain refinement. Ultra fine grained Mg alloys with grain size around 100 nm were successfully prepared by high-pressure torsion. Ultra-fine-grained structure can enhance diffusivity of alloying elements due to the significant volume fraction of grain boundaries. As a consequence, precipitation effects in ultra-fine-grained alloys may occur faster than in corresponding coarse-grained materials. This phenomenon was examined in this work by comparison of the precipitation sequence in Mg–Tb–Nd and Mg–Gd alloys with ultra-fine-grained structure and corresponding coarse-grained alloys.

Keywords: Positron annihilation; Mg alloys; High-pressure torsion; Precipitation hardening

1. Introduction

Mg–Gd and Mg–Tb–Nd systems are novel Mg-based light hardenable alloys with a high creep resistance at elevated temperatures. The supersaturated solid solution (sss) in these alloys decomposes in the following sequence of successive phases:

(i) Mg–Gd [1, 2]: sss → β″ ($D0_{19}$) → β′ (cbco) → β (fcc, Mg_5Gd, stable);

(ii) Mg–Tb–Nd [3]: sss → β″ ($D0_{19}$) → β_1 (fcc) → β (cubic, stable).

Mechanical properties of these alloys could be improved by grain refinement achieved by severe plastic deformation. Ultra-fine-grained (UFG) Mg–Gd and Mg–Tb–Nd alloys were successfully prepared by high-pressure torsion (HPT) [4]. In the present work we studied the influence of the UFG structure on the decomposition of sss. In general, two processes take place with increasing temperature in UFG alloys: (i) recovery of defects, and (ii) decomposition of sss. It is important to know how the precipitation sequence is influenced by the UFG structure. To examine it we compared precipitation effects in solution-treated (coarse-grained) and HPT-deformed alloys.

A high number of defects created in the course of HPT processing influences the precipitation effects in UFG materials. In this work we employed positron lifetime (PL) spectroscopy which represents a well developed non-destructive technique with a high sensitivity to open volume defects (e.g. vacancies, dislocations etc.) [5]. It enables determination of the nature of defects and of defect concentrations in the studied materials. PL spectroscopy was combined with transmission electron microscopy (TEM), electrical resistivity, and Vickers microhardness (HV) measurements.

2. Experimental details

Mg-3 wt.% Tb-2 wt.% Nd (Mg3Tb2Nd) and Mg-9 wt.% Gd (Mg9Gd) alloys with chemical composition shown in Table 1 were prepared by squeeze casting and subjected to 6 h solution annealing at 525 °C and 500 °C, respectively, to dissolve the alloying elements in the Mg matrix [1, 6]. The UFG structure was fabricated by HPT at room temperature using 5 rotations under a pressure of 6 GPa. Precipitation effects were studied on specimens subjected to isochronal annealing (20 K/20 min).

A fast–fast PL spectrometer [7] with time resolution of 160 ps was used in this work. At least 10^7 annihilation events were accumulated in each PL spectrum using a ≈ 1 MBq ^{22}NaCl positron source on 2 μm thick mylar foil. TEM observations were carried out on a JEOL JEM 2000 FX electron microscope operating at 200 kV. Relative electrical resistivity changes $\Delta\rho/\rho_0$ were measured using the dc four-point method with a dummy specimen in series. The influence of parasitic thermo-electromotive forces was

Table 1. Chemical analysis of the studied alloys. Concentrations are given in wt.%.

Material	Gd	Tb	Nd	Mn	Fe	Zn	Al	Si	Cu	Ni	Mg
Mg3Tb2Nd	–	3.15	1.75	0.014	0.020	0.0001	0.0077	0.0090	0.0026	0.0004	balance
Mg9Gd	9.33	–	–	0.014	0.020	0.0001	0.0077	0.0090	0.0026	0.0004	balance

Table 2. Results of PL measurements for Mg3Tb2Nd and Mg9Gd alloys in the solution-treated and HPT-deformed state and in important annealed states corresponding to local maxima in the relative intensity I_2. The mean positron lifetime and the lifetime $\tau_{1,STM}$ calculated in the frame of the two-state trapping model using Eq. (1) are shown in the last two columns.

Sample	τ_1 (ps)	I_1 (%)	τ_2 (ps)	I_2 (%)	τ_{mean} (ps)	$\tau_{1,STM}$ (ps)
Mg3Tb2Nd						
solution treated	225 ± 1	100	–	–	225 ± 1	–
β_1, T = 340 °C	150 ± 9	16.2 ± 0.6	252 ± 4	83.8 ± 0.6	235 ± 1	145 ± 6
HPT-deformed	90 ± 9	6.2 ± 0.8	251 ± 2	93.8 ± 0.8	241 ± 1	88 ± 4
HPT-deformed, β_1, T = 260 °C	205 ± 5	39 ± 3	250 ± 4	61 ± 3	232 ± 1	195 ± 5
Mg9Gd						
solution-treated	210 ± 3	91 ± 1	301 ± 2	9 ± 1	218 ± 1	214 ± 2
β″, T = 120 °C	204 ± 1	71 ± 1	300 ± 5	30 ± 2	232 ± 1	198 ± 2
β′-1, T = 220 °C	221 ± 2	89 ± 4	256 ± 4	11 ± 2	225 ± 1	216 ± 2
β′-2, T = 300 °C	214 ± 2	87 ± 3	250 ± 5	13 ± 2	219 ± 1	216 ± 2
HPT-deformed	180 ± 3	34 ± 2	256 ± 3	66 ± 2	230 ± 1	182 ± 3
HPT-deformed, β″, T = 100 °C	185 ± 3	32 ± 2	249 ± 4	68 ± 2	229 ± 1	187 ± 3
HPT-deformed, β, T = 300 °C	214 ± 2	60 ± 3	250 ± 3	40 ± 1	228 ± 1	211 ± 3

suppressed by current reversal. The Vicker's microhardness, HV, was measured by a STRUERS Duramin 300 hardness tester using a load of 100 g applied for 10 s.

3. Results and discussion

The PL results for the solution-treated specimens and HPT-deformed specimens are shown in Table 2. The solution-treated Mg3Tb2Nd alloy exhibits a single-component spectrum with a lifetime consistent with the bulk positron lifetime τ_B = 225 ps in well annealed pure Mg [2]. Thus, this sample exhibits very low defect density and may be considered as a defect-free material. The solution-treated Mg9Gd alloy contains additionally a weak component with a lifetime of ≈ 300 ps which comes from quenched-in vacancies bound to Gd atoms [2]. From the sensitivity threshold of PL spectroscopy one can deduce that the dislocation density in both solution-treated alloys does not exceed 10^{12} m^{-2} in accordance with optical metallography and TEM studies which revealed coarse grains with size in the range 100–500 μm and a low dislocation density.

TEM micrographs of HPT-deformed alloys (Fig. 1a and b) show a UFG structure with a grain size of ≈ 100 nm and a high dislocation density. PL spectra of HPT-deformed alloys consist of (i) a short-lived component with lifetime $\tau_1 < \tau_B$, which represents a contribution of free, delocalized positrons, and (ii) a dominant contribution with lifetime $\tau_2 \approx 256$ ps arising from positrons trapped at dislocations [8]. The lifetime

$$\tau_{1,STM} = \frac{1 - I_2}{\frac{1}{\tau_B} - \frac{I_2}{\tau_2}} \quad (1)$$

was calculated in order to check consistency of the decomposition of PL spectra with the two-state simple trapping model (STM) [5]. One can see in Table 2 that there is a reasonable agreement of $\tau_{1,STM}$ with the lifetime τ_1 of the short-lived component. This testifies that assumptions of the two-state STM (single type of defects, uniform distribution of defects, no detrapping etc.) are fulfilled in all studied specimens.

Figure 2a and b, respectively, show the temperature dependences of lifetimes τ_1 and τ_2 of the exponential components resolved in PL spectra of the solution-treated Mg3Tb2Nd and Mg9Gd alloys. One can see in these figures that the behaviour of the short-lived component lifetime τ_1 is consistent with the two-state STM, which is demonstrated by a good agreement of τ_1 with $\tau_{1,STM}$ calculated using Eq. (1) at all annealing temperatures. The temperature dependences of HV, electrical resistivity, and intensity

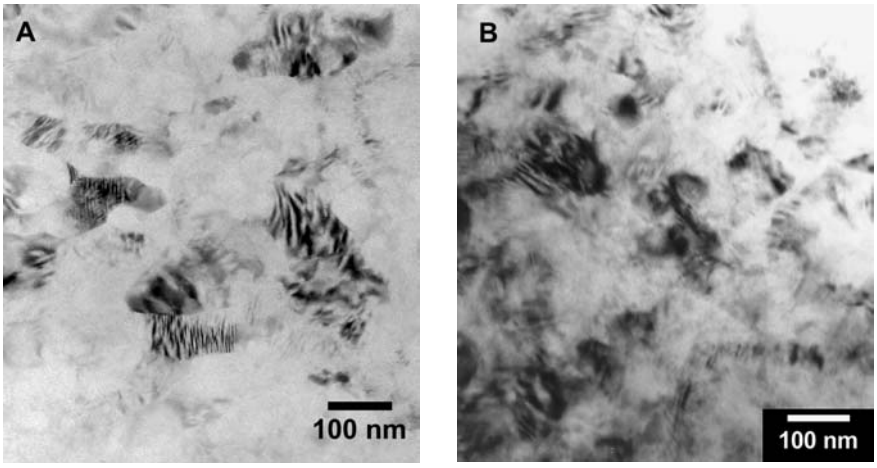

Fig. 1. Representative TEM micrographs of HPT-deformed (a) Mg3Tb2Nd and (b) Mg9Gd alloys.

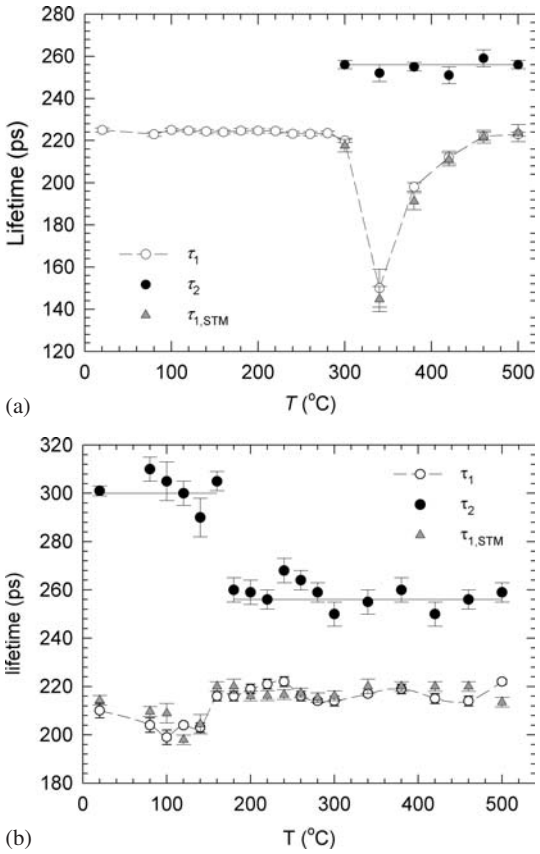

Fig. 2. Temperature dependence of lifetimes τ_1 and τ_2 of the exponential components resolved in PL spectra of solution-treated specimens (a) Mg3Tb2Nd, and (b) Mg9Gd. The lifetime $\tau_{1,STM}$ calculated according to the two-state STM using Eq. (1) is included in the figures as well.

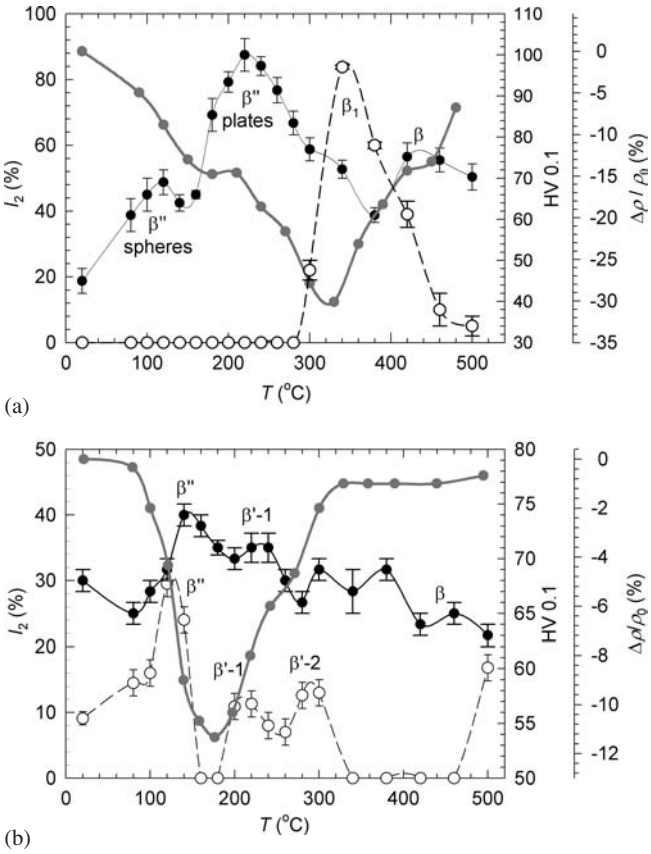

Fig. 3. Temperature dependence of HV (full black circles), electrical resistivity $(\rho-\rho_0)/\rho_0$ (grey circles), and intensity I_2 of trapped positrons (open circles) for solution treated specimens of (a) Mg3Tb2Nd, and (b) Mg9Gd.

I_2 of positrons trapped at defects in solution-treated Mg3Tb2Nd and Mg9Gd alloys are plotted in Fig. 3a and b, respectively. PL results of selected states corresponding to annealing temperatures where I_2 exhibits a local maximum are collected in Table 2. The decomposition sequence in solution-treated Mg3Tb2Nd starts by precipitation of the β″ phase at ≈ 80 °C. The β″-phase particles are fully coherent with the Mg lattice and do not contain any open volume defects capable of positron trapping. Thus, there are no active positron traps and up to 280 °C all positrons annihilate from the free state ($I_2 = 0$). Very small spherical particles of β″-phase formed at the beginning transform into fine plates in the temperature interval (160–240) °C. Figure 3a shows that fine plates (15–30 nm) of β″-phase have a strong hardening effect with a peak hardness at 220 °C. Further annealing up to 280 °C leads to a growth of the precipitates reflected by a decrease in HV. Note that very weak diffraction spots observed at 270 °C indicate that the β″-phase coexists with traces of the c base centred orthorhombic (cbco) β′-phase at this temperature [3]. As the volume fraction of the β′-phase is very low it is not considered in the further interpretation. Above 280 °C the β″-phase transforms into the β_1-phase. Plates (≈ 600 nm in diameter) of the β_1-phase were observed by TEM at 330 °C. Figure 3a shows that β_1-particles have a very strong effect on the electrical resistivity and PL spectra. Precipitation of β_1 causes a steep rise of a defect component with lifetime $\tau_2 \approx 256$ ps. The intensity I_2 of this component achieves a maximum at 340 °C. Thus, vacancy-like defects are created by formation of semi coherent β_1-phase precipitates. Positrons are likely trapped at misfit defect, i.e. open volumes existing at the precipitate-matrix interfaces due to lattice mismatch. The stable β-phase precipitates from 400 °C and also causes a noticeable hardening. Above 450 °C the solid solution is restored.

Figure 4a and b, respectively, show the temperature dependences of positron lifetimes τ_1 and τ_2 for HPT-deformed Mg3Tb2Nd and Mg9Gd. The temperature dependences of HV and I_2 for HPT-deformed Mg3Tb2Nd are plotted in Fig. 5a. The strong decrease in I_2 in the temperature range (100–160) °C is caused by recovery of dislocations. Maximum hardening is caused again by the precipitation of fine plates of coherent β″-phase. One can see in Fig. 5a that the intensity I_2, belonging to trapped positrons, starts to increase in the HPT-deformed sample annealed up to 200 °C and reaches its maximum at 260 °C. This increase occurs due to positron trapping at misfit defects introduced by precipitation of the semi-coherent β_1-phase. Figure 6a shows a TEM image of HPT-deformed Mg3Tb2Nd annealed up to 240 °C which contains fine (≈ 10 nm) plates of β_1-phase. After annealing above 260 °C, the behaviour of I_2 is reversed and it gradually decreases due to coarsening of β_1-particles. Thus, precipitation of the semi-coherent β_1-phase in the HPT-deformed alloy starts at substantially lower temperatures compared to the solution-treated alloy.

The quenched-in vacancies bound to Gd atoms in the solution-treated Mg9Gd alloy facilitate diffusion of Gd atoms and are subsequently incorporated in the coherent β″-parti-

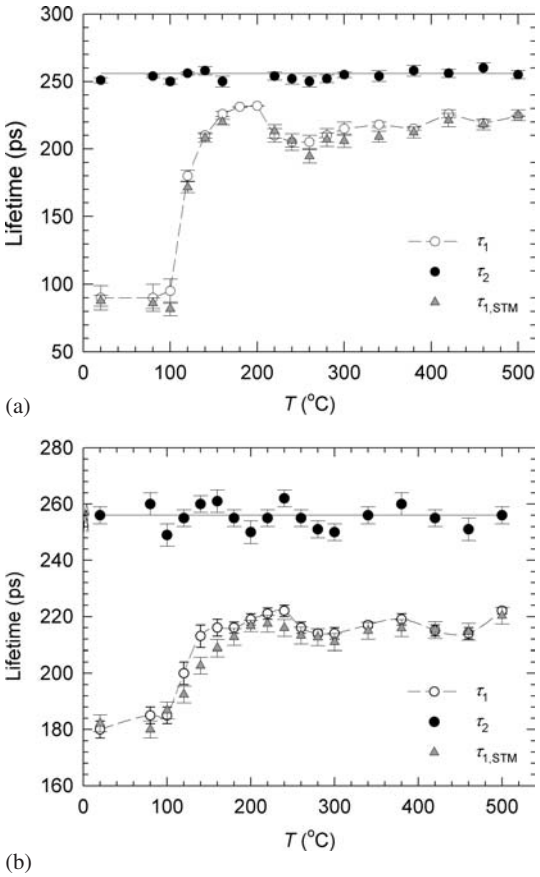

Fig. 4. Temperature dependence of lifetimes τ_1 and τ_2 of the exponential components resolved in PL spectra of HPT-deformed specimens (a) Mg3Tb2Nd, and (b) Mg9Gd. The lifetime $\tau_{1,STM}$, calculated using Eq. (1), is plotted in the figures as well.

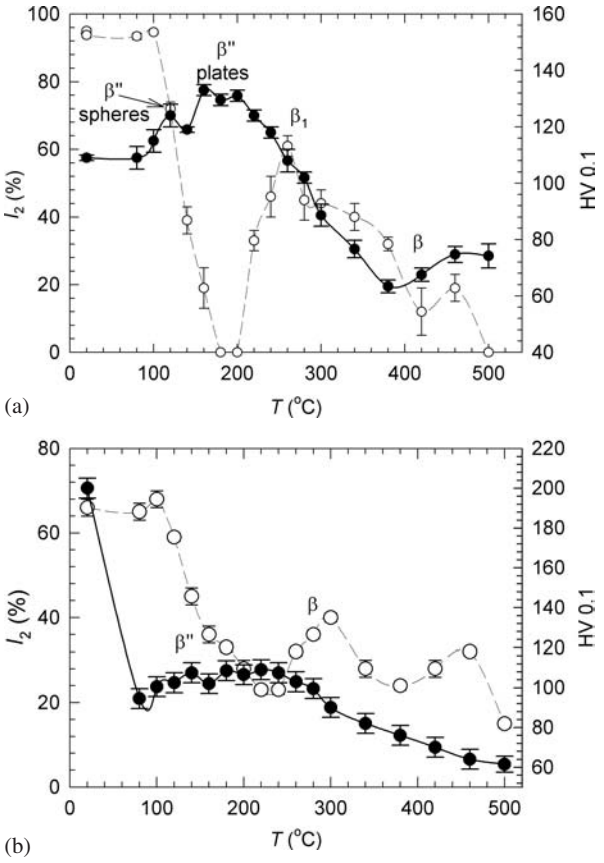

Fig. 5. Temperature dependence of HV (solid black circles) and intensity I_2 of trapped positrons (open circles) for HPT deformed specimens of (a) Mg3Tb2Nd and (b) Mg9Gd.

cles formed above 80 °C. The presence of open-volume defects in the β″-particles is testified by positron trapping at these precipitates seen as an increase of I_2 in the temperature range (80, 120) °C. At higher temperatures the β″-particles coarsen and the associated vacancies are annealed out causing a drop in I_2. The fine β″-particles cause a noticeable hardening (≈ 10 %). At 200 °C the β″-phase transforms into the semi-coherent β′-phase (denoted here as β′-1) precipitating as fine plates on the {2110} planes in all three possible orientation modes [1]. Positrons are trapped in misfit defects at the semi-coherent interfaces. Above 260 °C two of the orientation modes dissolve whereas the particles of the remaining mode (denoted here as β′-2) grow into oval plates with a diameter of about 100 nm [1]. This explains the two-peak character of I_2 and HV dependences. Finally, above 350 °C coarse spherical precipitates of the stable β-phase are formed and above 450 °C the solid solution is restored.

Recovery of dislocations in the HPT-deformed Mg9Gd alloy causes a drastic decrease in I_2 and HV at low temperatures in a similar manner as in the HPT-deformed Mg3Tb2Nd alloy. Nevertheless, a local increase in I_2 can

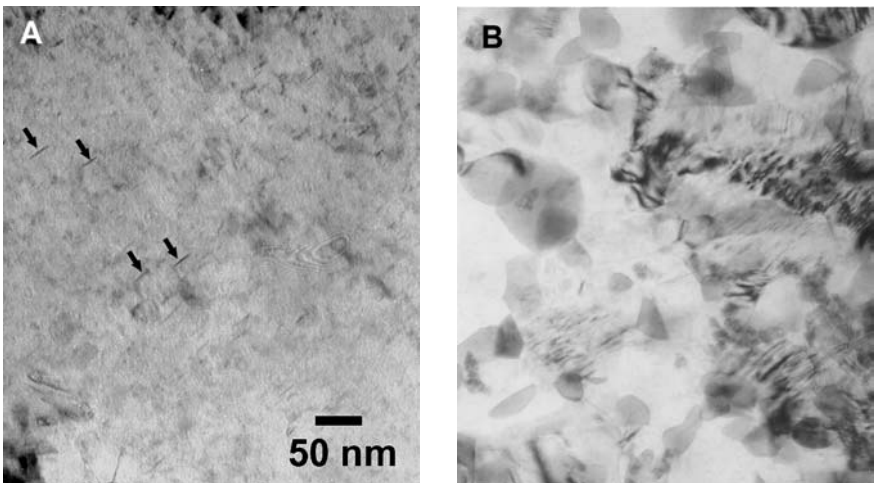

Fig. 6. TEM micrographs of annealed HPT-deformed alloys: (a) HPT-deformed Mg3Tb2Nd alloy annealed up to 240 °C containing fine plates of semicoherent β_1-phase (some of them are indicated by arrows); (b) HPT-deformed Mg9Gd alloy annealed up to 300 °C with precipitates of stable β-phase.

Table 3. Summary of precipitation effects in solution-treated and HPT-deformed alloys. All temperatures are given in °C.

Mg3Tb2Nd	β″ spheres (D019)	β″ plates (D019)	β_1 (fcc)	β (cubic)	peak hardening
solution- treated	80–160	160–280	280–400	400–450	220 (β″)
HPT- deformed	80–140	140–200	200–380	380–450	160 (β″)

Mg9Gd	β″ (D019)	β′-1 (c-bco)	β′-2 (c-bco)	β (fcc)	peak hardening
solution- treated	80–200	200–260	260–350	350–450	140 (β″)
HPT- deformed	80–160	160–240		240–450	240 (β)

be seen at 100 °C; similarly HV starts to increase slightly at 100 °C indicating formation of the β″-phase. Thus, in the temperature range (100, 220) °C two competitive processes take place in the HPT-deformed Mg9Gd specimen: (i) precipitation hardening caused by the β″-particles and (ii) softening due to the recovery of dislocations. At 260 °C I_2 starts to increase again accompanied by an additional slight hardening. This testifies to precipitation of a new phase. A maximum of I_2 is attained at 300 °C. The TEM observations at this temperature (see Fig. 6b) revealed precipitates of the stable β-phase. Coarsening of the β-phase precipitates above 300 °C leads to a subsequent decrease of I_2.

Table 3 compares precipitation effects observed in solution-treated and HPT-deformed alloys. Precipitation is accelerated in HPT-deformed specimens. For example, precipitation of the β_1-phase in HPT-deformed Mg3Tb2Nd is shifted by about of 80 K to lower temperatures and precipitation of the β-phase in Mg9Gd is shifted by about of 110 K to lower temperatures. This acceleration of precipitation indicates that diffusivity of the alloying elements in the UFG alloy is enhanced due to a high fraction of grain boundaries. It should be mentioned that grain growth in both HPT-deformed alloys was observed only at 300 °C. Hence, the UFG structure in HPT-deformed Mg3Tb2Nd and Mg9Gd exhibits an excellent thermal stability.

4. Summary

Precipitation effects in coarse-grained and UFG Mg3Tb2Nd and Mg9Gd alloys were compared. It was found that the UFG structure influences decomposition of the supersaturated solid solution. A general trend is a shift of the precipitation to lower temperatures. The precipitation effects are facilitated in UFG alloys due to (i) the extremely small grain size which leads to a significant volume fraction of grain boundaries acting as nucleation centres for the second-phase particles, and (ii) enhanced diffusivity of the alloying elements by the a possibility to diffuse along grain boundaries.

This work was supported the Ministry of Education of The Czech Republic (project MS 0021620834) and The Academy of Science of The Czech Republic (project KAN300100801).

References

[1] P. Vostrý, B. Smola, I. Stulíková, F. von Buch, B.L. Mordike: phys. stat. sol. (a) 175 (1999) 491–500.
[2] J. Čížek, I. Procházka, B. Smola, I. Stulíková: phys. stat. sol. (a) 203 (2006) 466–477.
[3] V. Neubert. I. Stulíková, B. Smola, B.L. Mordike, M. Vlach, J. Pelcová: Mater. Sci. Eng. A 462 (2007) 329–333.
[4] R.Z. Valiev, R.K. Islamgaliev, I.V. Alexandrov: Prog. Mater. Sci. 45 (2000) 103–189.
[5] P. Hautojärvi, C. Corbel, in: A. Dupasquier, A.P. Mills (Eds.), Proceedings of the International School of Physics "Enrico Fermi", Course CXXV, IOS Press, Varena (1995) 491–511.
[6] J. Čížek, I. Procházka, B. Smola, I. Stulíková, M. Vlach, R.K. Islamgaliev, O. Kulyasova, in: K.U. Kainer (Ed.), Magnesium 2006, Proceedings of the 7th International Conference on Magnesium Alloys and Their Applications, Wiley-VCH, Weiheim (2007) 517–522.
[7] F. Bečvář, J. Čížek, L. Lešták, I. Novotný, I. Procházka, F. Šebesta: Nucl. Instr. Meth. A 443 (2000) 557–577.
[8] J. Čížek, I. Procházka, B. Smola, I. Stulíková, V. Ocenášek: J. Alloys and Comp. 430 (2007) 92–96.

(Received August 28, 2008; accepted April 2, 2009)

Bibliography

DOI 10.3139/146.110103
Int. J. Mat. Res. (formerly Z. Metallkd.)
100 (2009) 6; page 780–784

ISSN 1862-5282

Correspondence address

Jakub Čížek
Faculty of Mathematics and Physics, Charles University
V Holešovičkách 2, CZ-180 00 Praha 8, Czech Republic
Tel.: +420 221 912 788
Fax: +420 221 912 567
E-mail: jakub.cizek@mff.cuni.cz

You will find the article and additional material by entering the document number **MK110103** on our website at *www.ijmr.de*